THE JOURNAL OF PHYSICAL CHEMISTRY Letters

Letter

Cite This: J. Phys. Chem. Lett. 2018, 9, 6179−6184

pubs.acs.org/JPCL

Optically Forged Diffraction-Unlimited Ripples in Graphene

Pekka Koskinen,*[,†] Karoliina Karppinen,[‡] Pasi Myllyperkiö,[‡] Vesa-Matti Hiltunen,[†] Andreas Johansson,[†,‡] and Mika Pettersson[‡]

[†]Nanoscience Center, Department of Physics, University of Jyväskylä, 40014 Jyväskylä, Finland

[‡]Nanoscience Center, Department of Chemistry, University of Jyväskylä, 40014 Jyväskylä, Finland

Supporting Information

ABSTRACT: In nanofabrication, just as in any other craft, the scale of spatial details is limited by the dimensions of the tool at hand. For example, the smallest details of direct laser writing with far-field light are set by the diffraction limit, which is approximately half of the used wavelength. In this work, we overcome this universal assertion by optically forging graphene ripples that show features with dimensions unlimited by diffraction. Thin sheet elasticity simulations suggest that the scaled-down ripples originate from the interplay between substrate adhesion, in-plane strain, and circular symmetry. The optical forging technique thus offers an accurate way to modify and shape 2D materials and facilitates the creation of controllable nanostructures for plasmonics, resonators, and nano-optics.

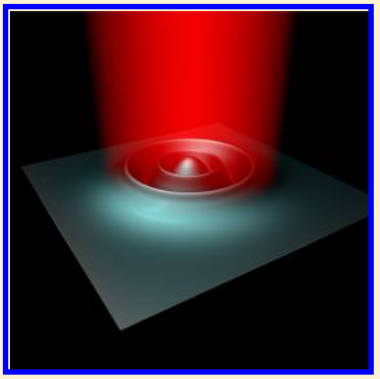

One of the central aims in nanoscience is to be able to modify nanostructures at will. Modifications are necessary because it is rarely the pristine materials but the modified and engineered materials that establish functionalities for practical applications.[1,2] Modifications are particularly necessary for 2D materials.[3,4] Graphene, for instance, gains specific functionalities once modified into ribbons,[5,6] introduced with pores or adsorbants,[7−10] or curved into 3D shapes.[11−13]

However, all modification techniques have their limitations. Direct mechanical manipulation is either slow and accurate,[14] or fast, coarse, and nonreproducible.[15,16] Thermal annealing,[17,18] electron irradiation,[19,20] chemical treatment,[21,22] and Joule heating[23] may be scalable but spatially imprecise due to their random character. It is particularly challenging to modify 2D materials into customized ripples and other 3D shapes. Such modifications frequently require dedicated experimental apparatuses[24] or specially prepared substrates.[25] The difficulty for 3D modification lies partly in substrate adhesion. Although often of weak van der Waals type, adhesion effectively prevents controlled detachment of 2D membranes from the substrate.

Limitations exist also in optical patterning. Although optical techniques may be scalable and easy to apply, the spatial details are determined by the size of the focused laser beam. Creating patterns with details finer than beam size is just as difficult as scribbling equations on a piece of paper with a spray can. Still, optical techniques have plenty of potential for exploration because irradiation provides various mechanisms to modify 2D materials, depending on laser energy and ambient atmosphere.[26,27] One particularly promising, still mostly untapped technique is the so-called optical forging, which alone enables controlled and on-the-fly 3D shaping of graphene.[28]

Given the ubiquity of various limitations, there is urgency to improve techniques to modify and engineer 2D materials scalably, accurately, and preferably in situ, without customized preparations.

In this work, we demonstrate optical forging of graphene into circular ripples with features much smaller than the size of the laser beam. By using thin sheet elasticity simulations, the rippling is shown to arise from the interplay between substrate adhesion, in-plane stress due to optical forging, and the underlying circular symmetry. Being based on direct irradiation of graphene without specially prepared experimental settings, optical forging provides a practical technique and thereby substantially broadens our abilities to modify and enhance the functionalities of graphene and maybe even other 2D materials.

To prepare the sample, we grew single-layer graphene by chemical vapor deposition (CVD) on a Cu substrate[29] and transferred it to thermally grown SiO_2. For fabrication details and graphene characterization, see the Supporting Information (SI).

Selected points in the sample were then irradiated by a 515 nm femtosecond laser focused with an objective lens (N.A. of 0.8) to a single Gaussian spot. To prevent photoinduced oxidation during the irradiation, the sample was installed inside a closed chamber purged with N_2.[27] The laser produced 250 fs pulses at 5−25 pJ/pulse energy and 600 kHz repetition rate for a tunable irradiation time τ. This process is called optical forging and results in blistering of the graphene membrane (Figure 1a and Movie 1 in the SI). Blistering occurs due to

Received: August 10, 2018
Accepted: October 11, 2018
Published: October 11, 2018

DOI: 10.1021/acs.jpclett.8b02461
J. Phys. Chem. Lett. 2018, 9, 6179−6184

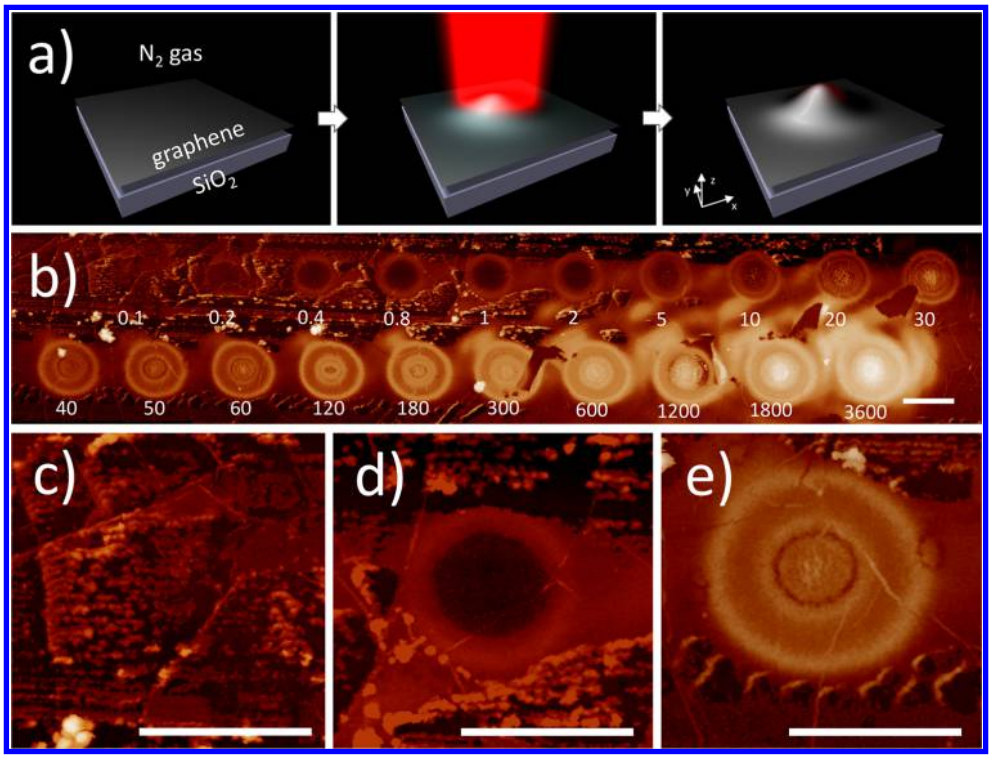

Figure 1. Monitoring the gradual formation of optically forged graphene blisters on SiO_2. (a) In optical forging, graphene is irradiated by focused femtosecond laser beam under an inert N_2 atmosphere. The laser creates defects that cause isotropic expansion of graphene membrane and trigger the formation of blisters. The blisters are hollow and not pressurized.[28] (b) Atomic force microscope image of blisters formed at progressively increasing irradiation time τ (numbers show τ in seconds; highest features are 60 nm). Blisters form at $\tau > 0.4$ s, initially with one circular ripple, later with several ripples and a dome in the center. (c) Zoom into an irradiated area with $\tau = 0.2$ s, where the graphene still remains flat. Visible are only the patchy residues from sample processing. (d) Zoom into a blister with one ripple ($\tau = 1$ s). (e) Zoom into a blister with multiple ripples ($\tau = 50$ s). Scale bars, 1 μm.

local expansion of the membrane, caused by laser-induced defects and the related compressive in-plane stress.[28] The local expansion field $\varepsilon(r)$ therefore depends on the time-integrated laser intensity profile $I(r)$, which enables accurate control over the expansion and blister height via the irradiation time τ. Consequently, we irradiated the sample at separate spots for irradiation times ranging from $\tau = 0.1$ to 3600 s. Finally, the blistered sample was characterized by Raman spectroscopy and measured by an atomic force microscope (AFM; see the SI).

The systematic increase in irradiation time produced a nontrivial but beautiful and reproducible pattern of blisters (Figure 1b and Figure S4). In particular, blisters had profiles more complex than the usual domes.[30] At short irradiation times ($\tau < 0.4$ s) the graphene remained flat on the substrate (Figure 1c). At intermediate irradiation times ($0.4 \leq \tau \leq 2$ s), the graphene developed blisters with one circular ripple (Figure 1d). At long irradiation times ($\tau \geq 5$ s) the graphene developed concentric ripples in progressively increasing numbers and a gradually developing central dome (Figure 1e and Movie 2 in the SI). Parts of the area between the blisters were detached from the substrate because the laser irradiated also during the movement from one spot to another. Note that the radial features in the ripples have dimensions down to 100 nm, nearly 10 times smaller than the laser spot and the ripple diameters themselves. Optical forging can thus reach 3D shaping of graphene that beats the diffraction limit. This is our main result.

To quantify the expansion of the graphene membrane, we used AFM height profiles to measure the increase in the surface area of the blisters. Within the projected areas of ~1 μm^2, the corrugated membrane areas increase nearly monotonously upon increasing irradiation time, reaching 10^{-2} μm^2 (~1%) area increase at $\tau = 1$ h (Figure 2a). Initially,

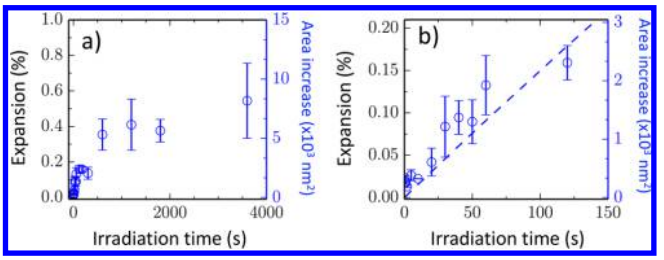

Figure 2. Effective expansion of graphene membrane during laser irradiation. (a) Area increase due to blister formation, as measured from the blister profiles of Figure 1b (right scale). Area increase transformed into maximum linear expansion in the middle of the laser spot (left scale). (b) Zoom into $\tau < 150$ s. A linear fit gives an expansion rate 1.5×10^{-3} %/s or 22 nm^2/s (dashed line). The vertical bars are uncertainties in blister areas.

the area increases linearly in irradiation time, at rate 22 nm^2/s (Figure 2b). This area increase was used to determine radius-dependent linear expansion, $\varepsilon(r)$. By assuming here a one-photon process and a Gaussian laser intensity profile $I(r)$, we obtain

$$\varepsilon(r) = \varepsilon_0 \exp(-4r^2 \log 2/\mathrm{fwhm}^2) \quad (1)$$

DOI: 10.1021/acs.jpclett.8b02461
J. Phys. Chem. Lett. 2018, 9, 6179−6184

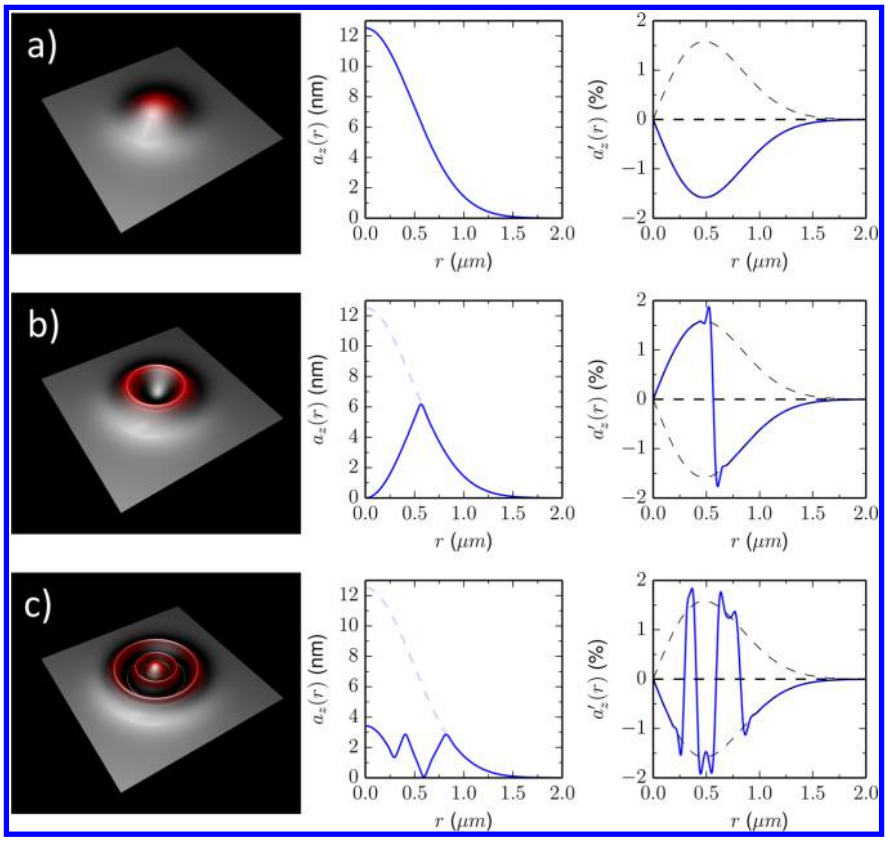

Figure 3. Thin sheet elasticity modeling of blisters with $\varepsilon_0 = 0.017\%$ and $\varepsilon_{adh} = 0$ (no substrate adhesion). (a) Blister with one central dome. (b) Blister with one circular ripple. (c) Blister with two concentric ripples and a central dome. Panels show visualizations (left; height exaggerated), radial height profiles $a_z(r)$ (middle), and the slopes of the radial height profiles $a_z'(r)$ (right). Dashed lines on the right show the analytical limits for $a_z'(r)$ from eq 3.

where $r = 0$ at the center of the spot and fwhm = 800 nm is the full width at half-maximum of the laser beam. Because the laser focal spot was difficult to maintain, fwhm had to be treated as a parameter and adjusted to give the best overall fit to the observed lateral dimensions in the experiment. The maximal expansion ε_0 increases at the rate 1.5×10^{-3} %/s at short irradiation times and saturates at almost 1% at long irradiation times (Figure 2). The initial linear rate and the saturation are in good agreement with previous experiments.[28]

The diffraction-unlimited rippling suggests a mechanism that involves competition between surface adhesion and expansion-induced stress. To investigate the mechanism in detail, we simulate blister growth by classical thin sheet elasticity model.[31] Such models have proven successful in the modeling of deformed graphene membranes.[16,32−36] The energy in the model contains in-plane strain energy, out-of-plane bending energy, and surface adhesion. The laser-induced isotropic expansion is introduced via the diagonal of the in-plane strain tensor as $e_{\alpha\beta}(\boldsymbol{r}) = e^0_{\alpha\beta}(\boldsymbol{r}) - \delta_{\alpha\beta}\varepsilon(\boldsymbol{r})$, where $\varepsilon(\boldsymbol{r})$ is the expansion field and $e^0_{\alpha\beta}(\boldsymbol{r})$ is the strain tensor of the unexpanded, pristine graphene.[28] The adhesion is modeled by the generic 12−6 Lennard-Jones potential.[37] This model was discretized, implemented in two computer codes (with and without circular symmetry), and used to optimize blister geometries for given ε_0 and adhesion energy ε_{adh}.[38] For details, see the SI.

Before analyzing the model in full, it is instructive first to ignore adhesion and calculate a few analytical results. Because of the smallness of the graphene bending modulus, on micrometer-length scales the mechanical behavior is dominated by in-plane strain energy.[39] The strain energy is minimized when $e_{\alpha\beta} \approx 0$ or $e^0_{\alpha\beta} \approx \delta_{\alpha\beta}\varepsilon(\boldsymbol{r})$. To a first approximation, eq 1 then implies an area increase of $\Delta A = [\pi/(2 \log 2)] \times \text{fwhm}^2\varepsilon_0$. (This relation was previously used to transform ΔA into ε_0.) With the displacement vector $\vec{a}(r) = a_r(r)\hat{r} + a_z(r)\hat{z}$, the diagonal components of the strain tensor become

$$\begin{cases} e_{rr}(r) = a_r'(r) + \dfrac{1}{2}[a_r'(r)^2 + a_z'(r)^2] - \varepsilon(r) \\ e_{tt}(r) = a_r(r)/r + \dfrac{1}{2}[a_r(r)/r]^2 - \varepsilon(r) \end{cases} \tag{2}$$

where r refers to radial and t refers to tangential in-plane component, and prime stands for a derivative with respect to r. Because the in-plane strain energy minimizes at $e_{\alpha\beta} \approx 0$, we obtain $a_r(r) \approx r\varepsilon(r)$ and

$$a_z'(r) \approx \pm\sqrt{16 \log 2 \times \varepsilon(r)}\,(r/\text{fwhm}) \tag{3}$$

That is, when the membrane adapts to isotropic expansion under radial symmetry, energy gets minimized by adjusting the slope into a fixed absolue value. When the slope is negative for all r, integration yields the profile $a_z(r) = \text{fwhm} \times \sqrt{\varepsilon(r)/\log 2}$. This profile corresponds to a blister with one central dome and a maximum height of $h_{max} = \text{fwhm} \times \sqrt{\varepsilon_0/\log 2}$. The numerically optimized blister profile follows this analytical estimate accurately (Figure 3a).

DOI: 10.1021/acs.jpclett.8b02461
J. Phys. Chem. Lett. 2018, 9, 6179−6184

However, positive and negative slopes in eq 3 are equally acceptable. Because the energy cost of bending is small, it is cheap to create a kink that reverses the sign of $a_z'(r)$ abruptly. This kink appears topologically as a perfectly round ripple (Figure 3b). Multiple kinks at different radii produce concentric ripples of varying heights and diameters (Figure 3c). Compared with the scale of in-plane strain energy, blisters of different ripple counts are nearly isoenergetic. When the number of ripples increases, the slopes progressively deviate from eq 3. Otherwise, the analytical description of the blister profiles without adhesion is apparent.

The role of adhesion, then, is to pull the membrane down, toward the substrate. Understanding the behavior of adhesion-free membranes is helpful, but when elastic and adhesive energies compete, we have to rely on numerical simulations. We took a closer look at the blister with τ = 1 s, which is near the onset of blistering (Figure 1d). This 4 nm high blister has a 0.97 μm ripple diameter and ε_0 = 0.017% expansion, as given by the AFM profile. We simulated this blister using the experimental ε_0 and adhesion in the range ε_{adh} = 0...1 eV/nm^2.

When ε_{adh} < 1 μeV/nm^2, the ripple is broad and the middle of the blister is mostly detached from the substrate, disagreeing with the experiment (Figure 4a); adhesion remains a minor perturbation to the zero-adhesion profile (Figure 3b). When ε_{adh} > 10 μeV/nm^2, in turn, the ripple becomes too narrow and shallow, also disagreeing with the experiment; when $\varepsilon_{adh} \gtrsim 100$ μeV/nm^2, the membrane ultimately snaps flat on the substrate. However, around $\varepsilon_{adh} \approx 3$ μeV/nm^2, adhesion pulls the membrane down so that both the ripple width and height agree with the experiment. Using the adhesion ε_{adh} = 3 μeV/nm^2, one-ripple blistering occurs at $\varepsilon_0 \approx 0.005\%$, and the blister height increases linearly when ε_0 further increases (Figure 4b). This simulated trend agrees with the experimental trend in one-ripple blisters ($\tau \lesssim 2$ s). These agreements suggest that the adhesion between laser-modified graphene and SiO_2 is observable but substantially smaller than typically observed for pristine van der Waals solids and clean interfaces.[40]

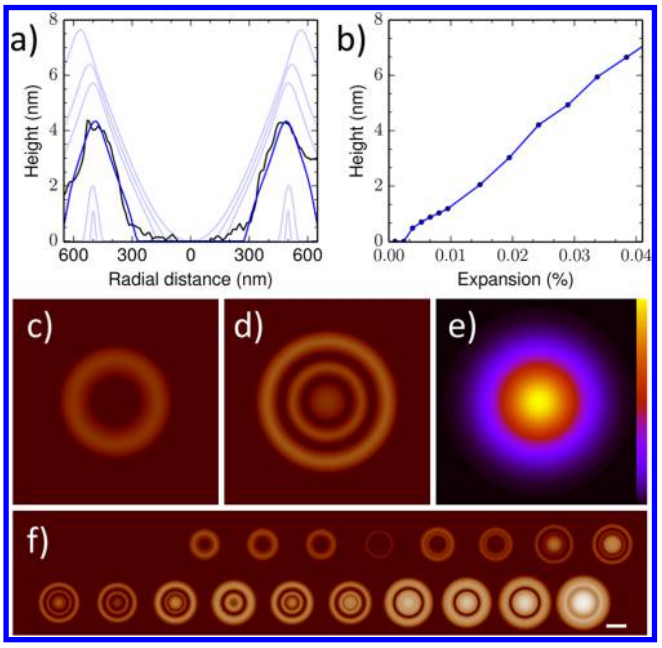

Figure 4. Thin sheet elasticity modeling of blisters with adhesion. (a) Experimental profile of τ = 1 s blister (black curve) compared with simulated profiles of one-ripple blisters with different adhesions (blue curves from top to bottom: ε_{adh} = 0, 0.5, 1.0, 3.0, 10, and 100 μeV/nm^2). (b) Height of one-ripple blister as a function of expansion ε_0. (c) Contour plot of a one-ripple blister with ε_0 = 0.017% (corresponding to τ = 1 s, Figure 1d). (d) Contour plot of a multiple-ripple blister with ε_0 = 0.09% (corresponding to τ = 50 s, Figure 1e). (e) Contour plot of $\varepsilon(r)/\varepsilon_0$ for all blisters. The color scale is linear from zero to one. (f) Contour plots for all energy-optimized blisters, using the expansions from Figure 2b and the initial guesses from Figure 1b. Scale bar, 1 μm. Field of view in panels c–e is 2.2 × 2.2 μm^2. Panels b–f have ε_{adh} = 3 μeV/nm^2, and all blisters are optimized without imposing radial symmetry.

Yet a question remains: Why do blisters initially appear with one circular ripple? This question can be addressed by considering eq 3. The preferred slope has a maximum at $r_0 = \text{fwhm}/2\sqrt{\ln 2} = 0.48$ μm. In other words, around radius r_0, the energy to keep the membrane flat is the largest. When the in-plane stress in a flat membrane increases upon increasing ε_0, it becomes energetically favorable to release the stress by creating the kink right at r_0 and making a circular ripple with diameter $2r_0$ = 0.96 μm. This result agrees well with the observations. Upon continuous irradiation, after the initial ripple has appeared, the ripple height increases until it becomes energetically favorable to create more ripples. This implies a process-dependent rippling of ever-increasing complexity.

This scenario for rippling was confirmed by performing global optimizations for blisters with ε_{adh} = 0.1–100 μeV/nm^2, ε_0 = 0.001...1%, and various types of initial guesses. First, at sufficiently small ε_0, the membrane remains flat without blistering. A critical limit for blistering is around $\varepsilon_0^c \approx 0.02 \times (\varepsilon_{adh}/\text{eV nm}^{-2})^{1/2}$. Second, when ε_0 increases just above the critical limit, the first blisters always have one ripple with diameter $D_0 \approx 1$ μm, independent of ε_{adh}. This result is in agreement with the experiments and with the maximum-slope argument given above ($D_0 \approx 2r_0$). Third, at intermediate values of ε_0, blisters show a complex pattern of ripples of varying heights and diameters. Fourth, at the limit of large ε_0, the in-plane strain energy dominates, and the minimum energy blisters always have one central dome (Figure 3a).

Compared with the typical magnitude of adhesion (1 to 2 eV/nm^2) between clean interfaces of van der Waals solids,[40−43] the adhesion in the model (~1 μeV/nm^2) is small. The smallness, however, is apparent even in a back-of-the-envelope calculation. Namely, upon blistering, the gain in elastic energy density is $k_s\varepsilon_0^2/(1-\nu)$, and the cost of adhesion energy density is ε_{adh}. At the onset of blistering, the two energies are equal, $\varepsilon_{adh} \approx k_s\varepsilon_0^2/(1-\nu)$. Because the blisters appear at $\varepsilon_0 \approx 0.02\%$, the adhesion has to be around 1–10 μeV/nm^2. The small adhesion may be due to water or functional groups,[44] topographic corrections,[45] electrostatics due to localized charge traps,[46] or other experimental details.[47,48] A detailed

DOI: 10.1021/acs.jpclett.8b02461
J. Phys. Chem. Lett. 2018, 9, 6179–6184

investigation of the laser-modified adhesion will be pursued later.

To summarize, by using the optical forging technique, we created diffraction-unlimited circular ripples in graphene on SiO_2. The rippling could be explained by the presence of circular symmetry amid the competition between substrate adhesion and in-plane compressive stress. In other words, the tiny rippling results spontaneously after creating an inhomogeneous expansion field on a much larger length scale. We can therefore straightforwardly predict that upon shrinking the size of the laser beam, the ripples will get smaller still. Once the mechanism responsible for the expansion of graphene is understood better, the technique could also be applied to other substrates and 2D materials. However, already now the technique and our observations provide many openings for novel research. A straightforward extension will be to control the rippling by engineering beam shapes. The technique produces beautiful circular blisters that probably have well-defined vibrational frequencies and can be used in resonators.[49] Via the formation of circular ripples, the technique also produced controllable curvatures that can be used to launch localized plasmons.[50] Thus, in addition to producing new physics and posing fundamental questions such as that of the laser-modified adhesion, the technique opens new avenues in the research of 2D materials.

■ ASSOCIATED CONTENT

Supporting Information

The Supporting Information is available free of charge on the ACS Publications website at DOI: 10.1021/acs.jpclett.8b02461.

Details of sample characterization and computer simulations (PDF)

Two movies illustrating the blister formation (ZIP)

■ AUTHOR INFORMATION

Corresponding Author

*E-mail: pekka.j.koskinen@jyu.fi.

ORCID

Pekka Koskinen: 0000-0001-7711-3562

Pasi Myllyperkiö: 0000-0003-1651-1676

Andreas Johansson: 0000-0003-0906-6287

Mika Pettersson: 0000-0002-6880-2283

Notes

The authors declare no competing financial interest.

■ ACKNOWLEDGMENTS

We acknowledge the Academy of Finland for funding (projects 297115 and 311330).

■ REFERENCES

(1) Stankovich, S.; Dikin, D. a.; Dommett, G. H. B.; Kohlhaas, K. M.; Zimney, E. J.; Stach, E. a.; Piner, R. D.; Nguyen, S. T.; Ruoff, R. S. Graphene-based composite materials. *Nature* **2006**, *442*, 282−286.

(2) Duong, D. L.; Yun, S. J.; Lee, Y. H. van der Waals Layered Materials: Opportunities and Challenges. *ACS Nano* **2017**, *11*, 11803.

(3) Geim, A. K.; Novoselov, K. S. The rise of graphene. *Nat. Mater.* **2007**, *6*, 183−191.

(4) Geim, A. K.; Grigorieva, I. V. Van der Waals heterostructures. *Nature* **2013**, *499*, 419−425.

(5) Son, Y.-W.; Cohen, M. L.; Louie, S. G. Half-metallic graphene nanoribbons. *Nature* **2006**, *444*, 347−349.

(6) Koskinen, P. Electromechanics of twisted graphene nanoribbons. *Appl. Phys. Lett.* **2011**, *99*, 013105.

(7) Gomes da Rocha, C.; Clayborne, P. A.; Koskinen, P.; Häkkinen, H. Optical and electronic properties of graphene nanoribbons upon adsorption of ligand-protected aluminum clusters. *Phys. Chem. Chem. Phys.* **2014**, *16*, 3558−3565.

(8) Zhao, J.; Deng, Q.; Bachmatiuk, A.; Sandeep, G.; Popov, A.; Eckert, J.; Rümmeli, M. H. Free-standing single-atom-thick iron membranes suspended in graphene pores. *Science* **2014**, *343*, 1228−1232.

(9) Koskinen, P.; Korhonen, T. Plenty of motion at the bottom: Atomically thin liquid gold membrane. *Nanoscale* **2015**, *7*, 10140.

(10) Antikainen, S.; Koskinen, P. Growth of two-dimensional Au patches in graphene pores: A density-functional study. *Comput. Mater. Sci.* **2017**, *131*, 120−125.

(11) Castro Neto, A. H.; Guinea, F.; Peres, N. M. R.; Novoselov, K. S.; Geim, A. K. The electronic properties of graphene. *Rev. Mod. Phys.* **2009**, *81*, 109−162.

(12) Levy, N.; Burke, S. a.; Meaker, K. L.; Panlasigui, M.; Zettl, A.; Guinea, F.; Neto, A. H. C.; Crommie, M. F. Strain-induced pseudo-magnetic fields greater than 300 T in graphene nanobubbles. *Science* **2010**, *329*, 544−547.

(13) Korhonen, T.; Koskinen, P. Electromechanics of graphene spirals. *AIP Adv.* **2014**, *4*, 127125.

(14) Eigler, D. M.; Schweizer, E. K. Positioning single atoms with a scanning tunneling microscope. *Nature* **1990**, *344*, 524.

(15) Kawai, T.; Okada, S.; Miyamoto, Y.; Hiura, H. Self-redirection of tearing edges in graphene: Tight-binding molecular dynamics simulations. *Phys. Rev. B: Condens. Matter Mater. Phys.* **2009**, *80*, 033401.

(16) Kit, O. O.; Tallinen, T.; Mahadevan, L.; Timonen, J.; Koskinen, P. Twisting Graphene Nanoribbons into Carbon Nanotubes. *Phys. Rev. B: Condens. Matter Mater. Phys.* **2012**, *85*, 085428.

(17) Chuvilin, A.; Kaiser, U.; Bichoutskaia, E.; Besley, N. A.; Khlobystov, A. N. Direct transformation of graphene to fullerene. *Nat. Chem.* **2010**, *2*, 450−453.

(18) Wang, D.; Chen, G.; Li, C.; Cheng, M.; Yang, W.; Wu, S.; Xie, G.; Zhang, J.; Zhao, J.; Lu, X.; et al. Thermally Induced Graphene Rotation on Hexagonal Boron Nitride. *Phys. Rev. Lett.* **2016**, *116*, 126101.

(19) Kotakoski, J.; Krasheninnikov, A. V.; Kaiser, U.; Meyer, J. C. From point defects in graphene to two-dimensional amorphous carbon. *Phys. Rev. Lett.* **2011**, *106*, 105505.

(20) Kotakoski, J.; Meyer, J. C.; Kurasch, S.; Santos-Cottin, D.; Kaiser, U.; Krasheninnikov, A. V. Stone-Wales-type transformations in carbon nanostructures driven by electron irradiation. *Phys. Rev. B: Condens. Matter Mater. Phys.* **2011**, *83*, 245420.

(21) Thompson-Flagg, R. C.; Moura, M. J. B.; Marder, M. Rippling of graphene. *EPL* **2009**, *85*, 46002.

(22) Svatek, S. A.; Scott, O. R.; Rivett, J. P. H.; Wright, K.; Baldoni, M.; Bichoutskaia, E.; Taniguchi, T.; Watanabe, K.; Marsden, A. J.; Wilson, N. R.; et al. Adsorbate-Induced Curvature and Stiffening of Graphene. *Nano Lett.* **2015**, *15*, 159−164.

(23) Jia, X.; Hofmann, M.; Meunier, V.; Sumpter, B. G.; Campos-Delgado, J.; Romo-Herrera, J. M.; Son, H.; Hsieh, Y.-P.; Reina, A.; Kong, J.; et al. Controlled formation of sharp zigzag and armchair edges in graphitic nanoribbons. *Science* **2009**, *323*, 1701−1705.

(24) Bao, W.; Miao, F.; Chen, Z.; Zhang, H.; Jang, W.; Dames, C.; Lau, C. N. Controlled ripple texturing of suspended graphene and ultrathin graphite membranes. *Nat. Nanotechnol.* **2009**, *4*, 562−566.

(25) Yamamoto, M.; Pierre-Louis, O.; Huang, J.; Fuhrer, M. S.; Einstein, T. L.; Cullen, W. G. "The Princess and the Pea" at the Nanoscale: Wrinkling and Delamination of Graphene on Nanoparticles. *Phys. Rev. X* **2012**, *2*, 041018.

(26) Aumanen, J.; Johansson, A.; Koivistoinen, J.; Myllyperkiö, P.; Pettersson, M. Patterning and tuning of electrical and optical properties of graphene by laser induced two-photon oxidation. *Nanoscale* **2015**, *7*, 2851−2855.

DOI: 10.1021/acs.jpclett.8b02461
J. Phys. Chem. Lett. 2018, 9, 6179−6184

(27) Koivistoinen, J.; Sladkova, L.; Aumanen, J.; Koskinen, P. J.; Roberts, K.; Johansson, A.; Myllyperkiö, P.; Pettersson, M. From Seeds to Islands: Growth of Oxidized Graphene by Two-Photon Oxidation. *J. Phys. Chem. C* **2016**, *120*, 22330.
(28) Johansson, A.; Myllyperkiö, P.; Koskinen, P.; Aumanen, J.; Koivistoinen, J.; Tsai, H. C.; Chen, C. H.; Chang, L. Y.; Hiltunen, V. M.; Manninen, J. J.; et al. Optical Forging of Graphene into Three-Dimensional Shapes. *Nano Lett.* **2017**, *17*, 6469−6474.
(29) Miller, D. L.; Keller, M. W.; Shaw, J. M.; Rice, K. P.; Keller, R. R.; Diederichsen, K. M. Giant secondary grain growth in Cu films on sapphire. *AIP Adv.* **2013**, *3*, 082105.
(30) Koenig, S. P.; Boddeti, N. G.; Dunn, M. L.; Bunch, J. S. Ultrastrong adhesion of graphene membranes. *Nat. Nanotechnol.* **2011**, *6*, 543−546.
(31) Landau, L. D.; Lifshitz, E. M. *Theory of Elasticity*, 3rd ed.; Pergamon: New York, 1986.
(32) Kudin, K.; Scuseria, G.; Yakobson, B. C2F, BN, and C nanoshell elasticity from ab initio computations. *Phys. Rev. B: Condens. Matter Mater. Phys.* **2001**, *64*, 235406.
(33) Shenoy, V.; Reddy, C.; Ramasubramaniam, A.; Zhang, Y. Edge-Stress-Induced Warping of Graphene Sheets and Nanoribbons. *Phys. Rev. Lett.* **2008**, *101*, 245501.
(34) Shenoy, V. B.; Reddy, C. D.; Zhang, Y.-W. Spontaneous curling of graphene sheets with reconstructed edges. *ACS Nano* **2010**, *4*, 4840−4844.
(35) Lambin, P. Elastic Properties and Stability of Physisorbed Graphene. *Appl. Sci.* **2014**, *4*, 282−304.
(36) Koskinen, P. Quantum Simulations of One-Dimensional Nanostructures under Arbitrary Deformations. *Phys. Rev. Appl.* **2016**, *6*, 034014.
(37) Koskinen, P. Graphene cardboard: From ripples to tunable metamaterial. *Appl. Phys. Lett.* **2014**, *104*, 101902.
(38) Bitzek, E.; Koskinen, P.; Gähler, F.; Moseler, M.; Gumbsch, P. Structural Relaxation Made Simple. *Phys. Rev. Lett.* **2006**, *97*, 170201.
(39) Korhonen, T.; Koskinen, P. Peeling of multilayer graphene creates complex interlayer sliding patterns. *Phys. Rev. B: Condens. Matter Mater. Phys.* **2015**, *92*, 115427.
(40) Björkman, T.; Gulans, A.; Krasheninnikov, A.; Nieminen, R. van der Waals Bonding in Layered Compounds from Advanced Density-Functional First-Principles Calculations. *Phys. Rev. Lett.* **2012**, *108*, 235502.
(41) Vanin, M.; Mortensen, J. J.; Kelkkanen, A. K.; Garcia-Lastra, J. M.; Thygesen, K. S.; Jacobsen, K. W. Graphene on metals: a Van den Waals density functional study. *Phys. Rev. B: Condens. Matter Mater. Phys.* **2010**, *81*, 081408.
(42) Hamada, I.; Otani, M. Comparative van der Waals density-functional study of graphene on metal surfaces. *Phys. Rev. B: Condens. Matter Mater. Phys.* **2010**, *82*, 153412.
(43) Tang, D.-M.; Kvashnin, D. G.; Najmaei, S.; Bando, Y.; Kimoto, K.; Koskinen, P.; Ajayan, P. M.; Yakobson, B. I.; Sorokin, P. B.; Lou, J.; et al. Nanomechanical cleavage of molybdenum disulphide atomic layers. *Nat. Commun.* **2014**, *5*, 3631.
(44) Gao, W.; Xiao, P.; Henkelman, G.; Liechti, K. M.; Huang, R. Interfacial adhesion between graphene and silicon dioxide by density functional theory with van der Waals corrections. *J. Phys. D: Appl. Phys.* **2014**, *47*, 255301.
(45) Delrio, F. W.; De Boer, M. P.; Knapp, J. A.; Reedy, E. D.; Clews, P. J.; Dunn, M. L. The role of van der Waals forces in adhesion of micromachined surfaces. *Nat. Mater.* **2005**, *4*, 629−634.
(46) Miwa, R. H.; Schmidt, T. M.; Scopel, W. L.; Fazzio, A. Doping of graphene adsorbed on the a-SiO2 surface. *Appl. Phys. Lett.* **2011**, *99*, 163108.
(47) Boddeti, N. G.; Liu, X.; Long, R.; Xiao, J.; Bunch, J. S.; Dunn, M. L. Graphene blisters with switchable shapes controlled by pressure and adhesion. *Nano Lett.* **2013**, *13*, 6216−6221.
(48) Miskin, M.; Sun, C.; Cohen, I.; Dichtel, W. R.; McEuen, P. Measuring and Manipulating the Adhesion of Graphene. *Nano Lett.* **2018**, *18*, 449.
(49) Bunch, J. S.; van der Zande, A. M.; Verbridge, S. S.; Frank, I. W.; Tanenbaum, D. M.; Parpia, J. M.; Craighead, H. G.; McEuen, P. L. Electromechanical Resonators from Graphene Sheets. *Science* **2007**, *315*, 490.
(50) Smirnova, D.; Mousavi, S. H.; Wang, Z.; Kivshar, Y. S.; Khanikaev, A. B. Trapping and Guiding Surface Plasmons in Curved Graphene Landscapes. *ACS Photonics* **2016**, *3*, 875−880.

DOI: 10.1021/acs.jpclett.8b02461
J. Phys. Chem. Lett. 2018, 9, 6179−6184